

Lattice dynamics and thermal transport of PbTe under high pressure

Ruihuan Cheng ^{1,*}, Xingchen Shen ^{2,*}, Stefan Klotz,³ Zezhu Zeng,¹ Zehua Li ^{2,4}, Alexandre Ivanov,⁵ Yu Xiao ⁶, Li-Dong Zhao ⁶, Frank Weber ^{2,†} and Yue Chen ^{1,‡}

¹*Department of Mechanical Engineering, The University of Hong Kong, Pokfulam Road, Hong Kong SAR, China*

²*Institute for Quantum Materials and Technologies, Karlsruhe Institute of Technology, 76021 Karlsruhe, Germany*

³*Institut de Minéralogie, de Physique des Matériaux et de Cosmochimie, CNRS UMR 7590,*

Sorbonne Université, 4 Place Jussieu, F-75252 Paris, France

⁴*Department of Inorganic Chemistry, Fritz-Haber-Institut der Max-Planck-Gesellschaft, Berlin 14195, Germany*

⁵*Institut Laue-Langevin, 71 Avenue des Martyrs CS 20156, 38042 Grenoble Cedex 9, France*

⁶*School of Materials Science and Engineering, Beihang University, Beijing 100191, China*



(Received 17 May 2023; revised 28 July 2023; accepted 29 August 2023; published 7 September 2023)

Understanding the high-pressure lattice dynamics is crucial to modulate the thermal transport in thermoelectric materials beyond the ambient environment. Herein, using molecular dynamics simulations in combination with an accurate machine-learning interatomic potential, we find the well-known double-peak feature of the transverse-optical (TO) mode in PbTe gradually vanishes when pressure is enhanced. An anomalous non-monotonic pressure dependence of the frequency of the transverse-acoustic phonon in PbTe is computationally reproduced. The longitudinal-acoustic, longitudinal-optical, and TO phonons harden as expected when pressure increases. The theoretical results are compared with inelastic neutron scattering experimental data. We have also calculated the pressure-dependent lattice thermal conductivity and revealed the phonon transport mechanisms.

DOI: [10.1103/PhysRevB.108.104306](https://doi.org/10.1103/PhysRevB.108.104306)

I. INTRODUCTION

Thermoelectric materials (TEs) pave a feasible way to convert low-grade heat into electricity, and have attracted great attention [1–4]. The energy conversion efficiency of TEs is evaluated by the dimensionless figure of merit $ZT = \sigma S^2 T / (\kappa_e + \kappa_L)$, where σ , S , κ_e , and κ_L correspond to the electrical conductivity, Seebeck coefficient, and electronic and lattice thermal conductivity at a specific temperature (T), respectively. While electrical properties (i.e., σ and S) are important to determine the performance of TEs and can be optimized through band engineering [5–9], lattice thermal conductivity (κ_L) is also critical. Thus, a deeper understanding of the lattice dynamics is conducive to better regulating the κ_L of TEs.

Lead telluride (PbTe), a NaCl-structure TE, has a low κ_L ($\sim 2.0 \text{ W m}^{-1} \text{ K}^{-1}$ at room temperature [10,11]) and its lattice dynamics have been extensively studied [12–27]. A first-principles study attributes the low κ_L of PbTe as well as other IV-VI compounds to the softening of optical phonon modes, strong anharmonic scattering, and large phase space of three-phonon scattering processes caused by resonant bonds [17]. Another study reveals that the low thermal conductivity of PbTe originates from three-phonon scattering through the transverse-optical (TO) phonon modes with large wave vectors around the Brillouin zone center [18]. Also, recent

research demonstrates that the four-phonon scattering processes lead to a significant reduction of κ_L [19]. On the other hand, the inelastic neutron scattering (INS) experiments show an anomalous double-peak TO phonon mode at zone center in PbTe [20–22]. The origin of this double-peak TO mode was also attributed to the strong phonon-phonon scattering, as revealed by theoretical studies [23,24]. Our recent work shows that the proximity to the incipient ferroelectric transition plays an important role in the origin of the double peak [25]. In addition, the strong anharmonic coupling between this ferroelectric TO and the longitudinal acoustic (LA) phonon modes in PbTe was also reported to contribute to its low thermal conductivity [14,15,26,27]. Despite the fact that many investigations have revealed the lattice dynamical properties of PbTe, these studies are based on ambient pressure and high-pressure lattice dynamics are not yet fully revealed due to the challenges of relevant INS experiments.

Herein, we systematically investigate the pressure-dependent lattice dynamics of PbTe under hydrostatic pressures up to 6 GPa using molecular dynamics (MD) simulations combined with machine-learning interatomic potential, which naturally involves full anharmonicity up to any arbitrary order [28]. With increasing pressure, our simulations show that the double-peak feature of the TO mode gradually disappears and the transverse-acoustic (TA) modes exhibit a softening trend. We also perform INS measurements that provide further experimental evidence. Moreover, the pressure-dependent κ_L is calculated to reveal the thermal transport mechanisms and provide a pressure dimension for regulating the κ_L of PbTe.

*These authors contributed equally to this work.

†frank.weber@kit.edu

‡yuechen@hku.hk

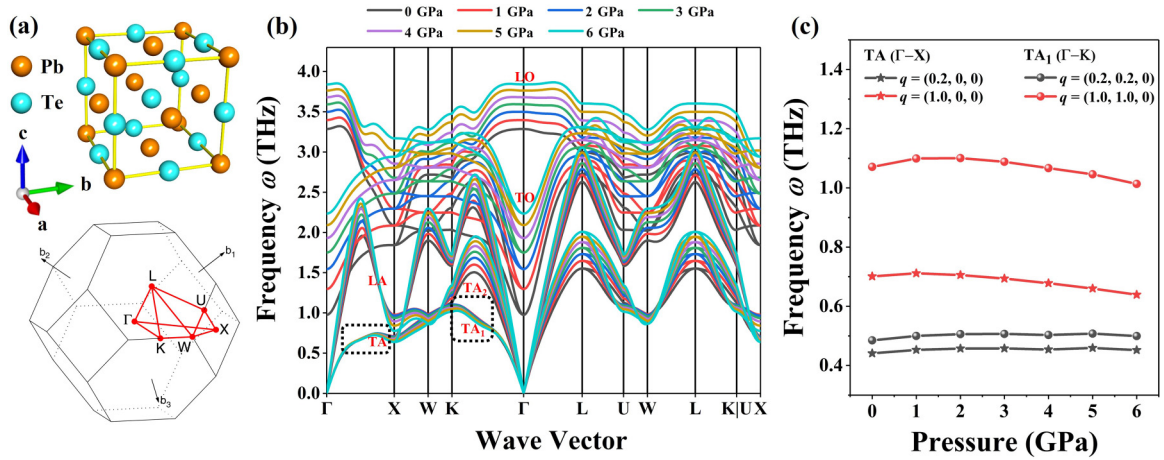


FIG. 1. (a) The rocksalt crystal structure of PbTe, and its reciprocal lattice space with high-symmetry points Γ , X, W, K, L, and U visualized using AFLOW [29]. (b) Harmonic phonon dispersions of PbTe under hydrostatic pressures from 0 to 6 GPa calculated through the finite-displacement method with our machine-learning NEP. (c) Frequency changes of selected TA modes under hydrostatic pressures along the Γ -X and K - Γ high-symmetry paths.

II. COMPUTATIONAL DETAILS

All the structural relaxation calculations were performed using the Vienna *Ab initio* Simulation Package (VASP) [30] within the framework of density functional theory (DFT) with a Γ -centering $13 \times 13 \times 13$ k -point mesh and a kinetic energy cutoff of 500 eV. The projector-augmented wave (PAW) method [31] was used in conjunction with the Perdew-Burke-Ernzerhof (PBE) generalized gradient approximation (GGA) for the exchange-correlation functional [32]. The force and energy convergence thresholds were set to 10^{-4} eV/Å and 10^{-8} eV, respectively. Phonon dispersions of PbTe under different pressures were calculated by extracting the harmonic interatomic force constants (IFCs) based on the finite-displacement approach using $4 \times 4 \times 4$ supercells (128 atoms).

The power spectra [$G_{qs}(\omega)$] of the mass-weighted atomic velocities were extracted from the MD trajectory using the normal-mode-decomposition technique as implemented in DYNAPHOPY [33,34]. The obtained $G_{qs}(\omega)$ were fitted to the Lorentzian function to extract the phonon frequencies and the corresponding anharmonic shifts. We used a $15 \times 15 \times 15$ supercell (6750 atoms) to perform MD simulations, which were firstly equilibrated in a Nosé-Hoover *NVT* ensemble for 100 ps, followed by *NVE* simulations of 1.2 ns to collect atomic trajectories with a time interval of 20 fs. All MD simulations based on our machine-learning neuroevolution potential (NEP) were performed using the graphics processing units molecular dynamics (GPUMD) package [35,36] with a time step of 1 fs.

III. EXPERIMENTS

The measurements reported here were performed at the 2T1 and IN8 [37,38] triple-axis spectrometers at the Laboratoire Léon Brillouin (LLB, Saclay) and the Institut Laue Langevin (ILL, Grenoble), respectively. Both are high-flux instruments located close to the reactor core (reactor hall) and are equipped with a focusing monochromator and analyzer

crystals. They are connected to thermal moderators. Most measurements were performed by constant- Q scans with a fixed final energy of 14.7 meV. The energy transfer is varied by scanning the energy of the incident neutrons. Both incident and scattered beams were constrained by two cadmium cones

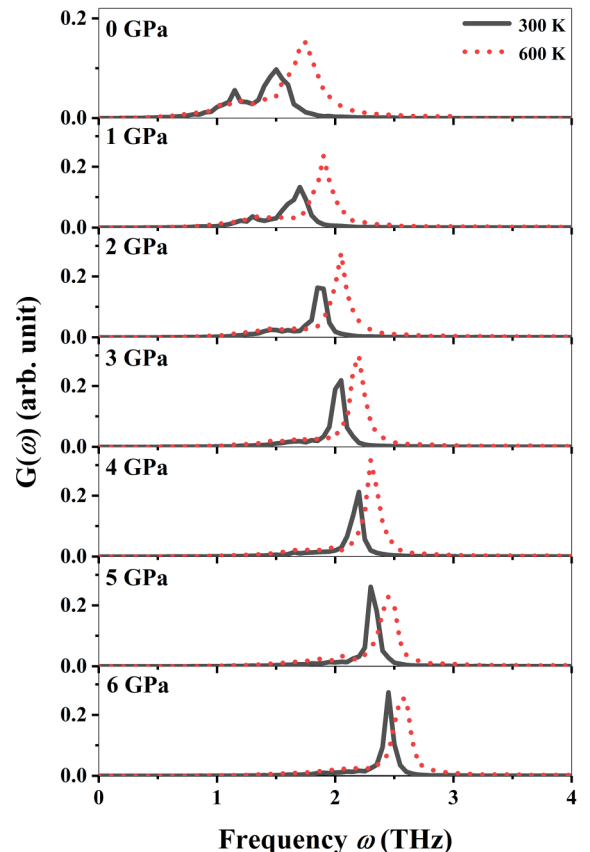


FIG. 2. Power spectra of the TO mode of PbTe at zone center under different hydrostatic pressures as calculated from MD simulations using the normal-mode-decomposition technique.

to minimize the background scattering from the pressure cell surrounding the sample. Single crystals of PbTe were pre-aligned in the 110-001 scattering plane to within 0.5° to avoid the need to tilt the pressure cell.

The single crystals in the LLB experiments were disks with a diameter of 4 mm and a thickness of 2 mm and were imbedded in lead which acts as a pressure transmitting medium. Tungsten carbide anvils with a toroidal profile and CuBe gaskets were used to compress the sample-gasket assembly. The required force of ~ 60 tonnes was provided by a four-column V3-type Paris-Edinburgh hydraulic press available at LLB. Details of this setup are given in Refs. [39,40]. The ILL experiment used a more recent and improved setup which allowed compression under strictly hydrostatic conditions using the 4:1 deuterated methanol-ethanol mixture which is known to stay fluid up to 10 GPa [39]. For this purpose, several PbTe samples were cut into disks with a 4 mm diameter and a 1.2 mm thickness and loaded in an encapsulating TiZr gasket [39] together with the pressure transmitting fluid. The samples were cut from one piece of single crystals which we already used in our recent study of PbTe phonons at ambient pressure [25]. The toroidal anvils in these measurements were made of zirconia-toughened alumina from Ceramtec (Plochingen, Germany) which ensures a significantly higher neutron transparency than tungsten carbide [41]. The gasket-anvil assembly was compressed with a two-column VX5 Paris-Edinburgh press available at ILL. The measurements [37,38] were performed with a flat monochromator and analyzer and $40'$ collimations to improve the momentum resolution.

IV. RESULTS AND DISCUSSION

A. Lattice dynamics from simulation

The crystal structure of PbTe is shown in Fig. 1(a). Figure 1(b) shows the harmonic phonon dispersions of PbTe under hydrostatic pressures from 0 to 6 GPa calculated using the finite-displacement method with machine-learning NEP (see Appendix A and Figs. 6–8 for more details of machine-learning NEP). When pressure increases from 0 to 6 GPa, the high-frequency optical phonon modes exhibit significant hardening along all of the high-symmetry paths. Similarly, the LA phonon modes also generally represent hardening features, except for the LA modes at the Brillouin zone boundary near the X point. Although the TA_2 modes show the expected hardening behavior along the Γ - L and Γ - K high-symmetry paths, the TA_1 phonon modes show an anomalous softening trend along the Γ - X and Γ - K high-symmetry paths [Figs. 1(b) and 1(c)].

One of the widely studied phonon features of PbTe is the double-peak power spectrum of the zone-center TO mode. Figure 2 shows the power spectra under different pressures calculated through MD simulations. The double-peak feature of the TO mode is observed at room temperature and 0 GPa, in agreement with previous calculations [21,23,25]. When the temperature is raised to 600 K, the intensity of the lower-energy peak is weakened. On the contrary, the intensity of the higher-energy peak is enhanced and it moves towards a higher frequency, and the overall spectral range is widened. At the same temperature, the spectra are incrementally dominated by

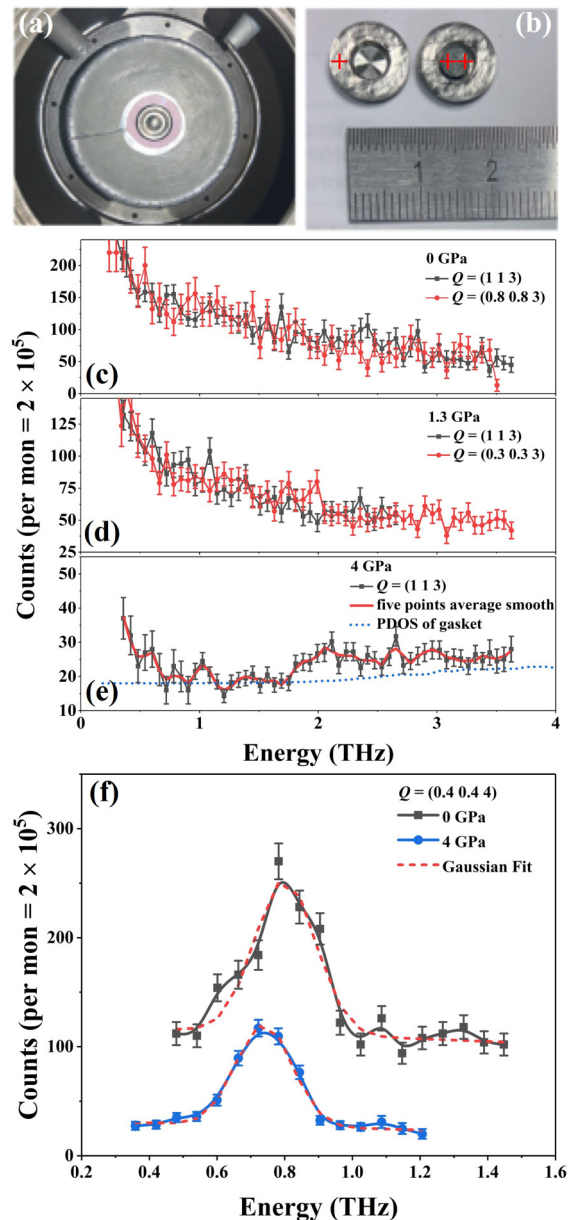


FIG. 3. (a) Assembled encapsulating metallic gasket containing the sample and the alcohol mixture. (b) Disassembled gasket (+) with the sample (++) in the center. Profile of the energy scans at zone center $Q = (1, 1, 3)$ at (c) 0 GPa, (d) 1.3 GPa, and (e) 4 GPa. The red solid line in (e) is the five points average smooth line, and the blue dashed line is the projected density of states (PDOS) of the gasket. (f) Profile of the energy scans for the TA_1 mode at $Q = (0.4, 0.4, 4)$ under ambient pressure and 4 GPa. The red dashed lines are Gaussian fits to the data.

a higher frequency weight with elevated pressure, indicating that the TO phonon in the center of the Brillouin zone shows a strong hardening feature. With the increase of pressure, the asymmetric spectral weight distribution gradually vanishes in PbTe at both 300 and 600 K, and the spectrum is dominated by a sharp feature when the pressure is above 3 GPa.

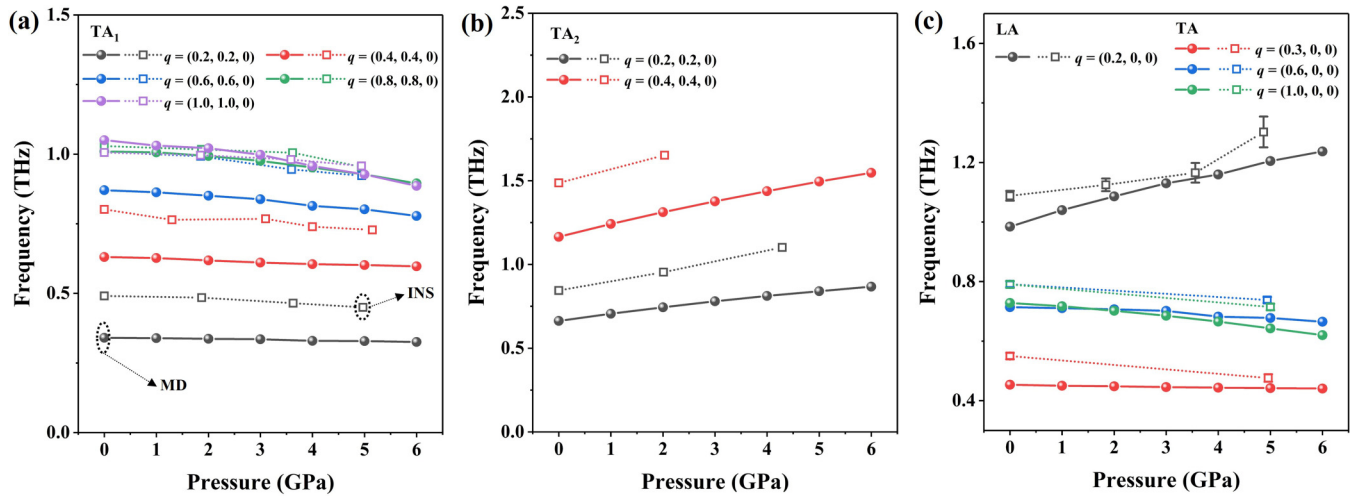


FIG. 4. Pressure-dependent phonon frequencies of the TA and LA modes at different q points along the (a),(b) Γ - K and (c) Γ - X high-symmetry paths, as obtained from inelastic neutron scattering (INS) experiments (hollow symbols) and from molecular dynamics (MD) simulations (solid symbols) with machine-learning NEP at 300 K through the normal-mode-decomposition technique. Part of the experimental data at 0 and 5 GPa are taken from Ref. [13]. Error bars of the INS results are shown but may be smaller than the symbol size. The lines are a guide to the eye.

B. Experimental observations

Phonon measurements were carried out through INS experiments under high pressures at room temperature. Figures 3(a) and 3(b) illustrate the experimental setup and the general predicament of such high-pressure experiments, respectively. The samples are limited to, for INS standards, rather small sizes whereas the neutron beam impinges not only on the sample but on a large amount of surrounding material, too. This yields a small signal, a large background, and an overall small signal-to-noise ratio. This is obvious in our data taken for the loaded but unpressurized cell [Fig. 3(c)] and in the data taken at small pressures [Fig. 3(d)]. The zone-center TO mode is known to have a room-temperature frequency of about 1 THz and it sharply disperses upwards going away from the zone center. Therefore, we performed energy scans away from the zone center [red data in Figs. 3(c) and 3(d)] in order to separate the background scattering from the phonon signal. However, it seems that the phonon signal is too small to be detected outside the statistical error bar of the background scattering. At higher pressures, the background decreases by a factor of up to 4 in the frequency range below 3 THz [Fig. 3(e)] [42]. The origin of this strong reduction of the intensity is currently not understood and the subject of further investigations. The reduced background allows a coarse analysis. By estimating an experimental background based on the phonon density of state of TiZr [43], the gasket material, the data show an increase above the background [blue dashed line in Fig. 3(e)] around a frequency of ~ 2 THz. Thus, our data indicate that the zone-center TO mode hardens to at least 2 THz at a pressure of 4 GPa, which is in agreement with our calculations (Fig. 2). However, the low data quality does not allow for an assessment of the peak shape.

On the other hand, scattering by acoustic phonons typically has a larger intensity, and thus can be detected more easily even on a large background. Furthermore, the measurements can be performed well away from the Bragg peak positions

[Fig. 3(f)]. Typically, we expect phonons to harden under pressure since lattice constants shrink and force constants between atoms increase. Indeed, we find this for several cases and discuss some of them in more detail below. Here, we highlight an unusual softening under pressure of the TA_1 mode propagating in the [110] direction [Fig. 3(f)]. This is in contrast to measurements of the corresponding elastic constants reporting a hardening but only up to 0.15 GPa [12].

C. Pressure dependence of phonon modes

Herein, our experimental results reveal an anomalous softening of the TA_1 mode under elevated pressure in PbTe [Fig. 3(f)]. In contrast, the TO [Figs. 3(c)–3(e)] and LA [Fig. 4(c)] modes harden when pressure increases. This softening trend of the TA mode was first reported by Klotz [13], who found that the TA mode showed a lower phonon frequency under pressure (below 5 GPa). Anderson and Liebermann pointed out that this softening behavior is generally in ionic compounds with NaCl structure and is related to the repulsive part of the interatomic potential [44].

The experimental and theoretical results show a consistent trend, i.e., the TA_1 modes along the Γ - K [Fig. 4(a)] and the degenerate TA modes along the Γ - X [Fig. 4(c)] high-symmetry paths soften with the increase of pressure, while the high-frequency TA_2 modes [Figs. 4(b) and 9(a)], LA modes [Fig. 4(c)], and the TA modes along the Γ - L [Fig. 9(b)] high-symmetry path harden with the increase of pressure. Although the theoretical phonon frequency is generally lower than the experimental value, the pressure dependencies are consistent. In our high-pressure experimental setup, the q resolution might become coarse, especially for smaller q vectors, leading to a notable phonon frequency difference between experiments and calculations. It is noted that the pressure dependence of TA_2 is generally stronger than that of TA_1 .

An early study based on ultrasonic experiments reported that the elastic constant C_{44} , related to one of the two TA

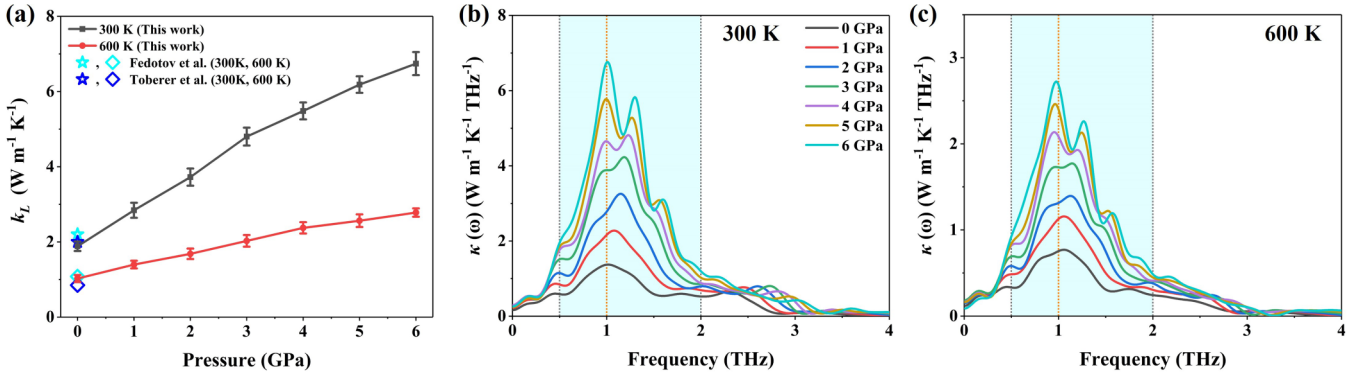


FIG. 5. (a) Lattice thermal conductivity of bulk PbTe as a function of pressure at 300 and 600 K, and the spectral lattice thermal conductivity (b),(c) calculated from HNEMD simulations with NEP. The experimental lattice thermal conductivities at 300 and 600 K [10,11] are also shown in (a) for comparisons.

phonons propagating along the [110] scattering plane as well as the TA mode along the [100] scattering plane, hardens under pressure [12]. However, the minimum pressure applied in our experiment (~ 2 GPa) is far greater than the maximum pressure (0.15 GPa) reported in Ref. [12]. Thus, a direct comparison of the experimental results cannot be made. On the other hand, the calculated harmonic phonons through the finite-displacement method show that when the pressure is lower than 1 GPa, the frequency of the related TA modes increases under pressure [Fig. 1(c)], which is consistent with the results reported in the literature [12,45].

D. Lattice thermal conductivity

Given that phonon properties directly dominate heat transfer in PbTe, we further computationally study the effect of pressure on the lattice thermal conductivity (κ_L). To obtain the κ_L of PbTe under various pressures, we carry out homogeneous nonequilibrium molecular dynamics (HNEMD) simulations [46–48] (see Appendix B and Fig. 11 for more details). Figure 5(a) shows the calculated κ_L of PbTe at 300 and 600 K under 0–6 GPa. We see that the κ_L under 0 GPa is consistent with ambient experimental data [10,11]. We find that with the increase of pressure, the κ_L of PbTe at 300 K monotonically increases from $1.9 \text{ W m}^{-1} \text{ K}^{-1}$ under 0 GPa to $6.8 \text{ W m}^{-1} \text{ K}^{-1}$ under 6 GPa. The monotonically increasing trend is also observed at 600 K, although the pressure dependence becomes weaker. This is mainly due to the enhanced phonon scatterings at high temperatures. We also note that in the framework of unified thermal transport theory [49], particlelike propagation dominates the thermal transport of PbTe, while the contribution of wavelike tunneling is found to be negligible as demonstrated by Zeng *et al.* [28].

The increasing trend of κ_L under pressure can be further understood based on the spectrum of thermal conductivity [$\kappa(\omega)$] as shown in Figs. 5(b) and 5(c). It is seen that phonons with frequency in the range from 0.5 to 2 THz contribute most to the thermal transport; within this range, the $\kappa(\omega)$ also increases significantly as pressure rises. Although the softened TA modes result in lower group velocities below 1.0 THz, the $\kappa(\omega)$ in this range still features an increasing trend. On the other hand, the avoided LA-TO crossing [Fig. 1(b)] caused by the rapid hardening of TO phonons under pressure and

the disappearance of the double peaks of the TO mode (see Fig. 2) suggest the weakening of phonon-phonon scatterings, which is conducive to the lattice heat transfer, thus leading to an increased value of κ_L . This is also evidenced by the rapid increase of $\kappa(\omega)$ between 1.0 and 2.0 THz, which dominates the overall enhancement of the lattice thermal conductivity under pressure.

V. CONCLUSION

In this work, the high-pressure lattice dynamics and thermal transport property of PbTe are thoroughly investigated. We find the double-peak feature of the TO mode at zone center gradually vanishes when pressure increases. The anomalous softening of the TA phonon modes under pressure is revealed by both MD simulations and INS measurements. We further demonstrate that the softening of the TA phonon modes does not suppress the phonon heat transfer, while the disappearance of the double peaks in the TO mode and the avoided LA-TO crossing likely play a more important role in the enhanced κ_L of PbTe under pressure. This work unveils the

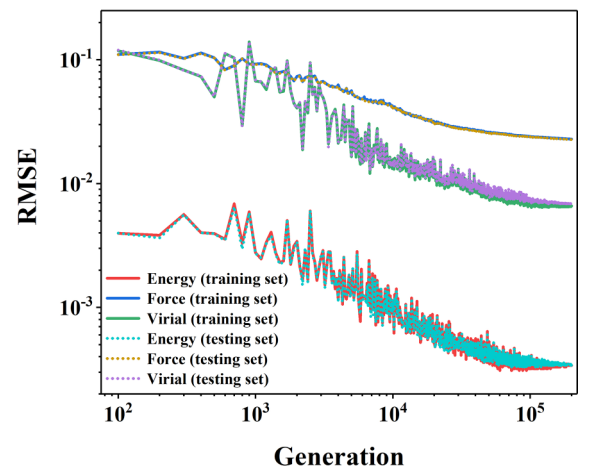


FIG. 6. Evolution of the energy, force, and virial root-mean-square errors (RMSEs) for both training and testing sets during the training process. The units of energy, force, and virial RMSEs are eV/atom, eV/Å, and eV/atom, respectively.

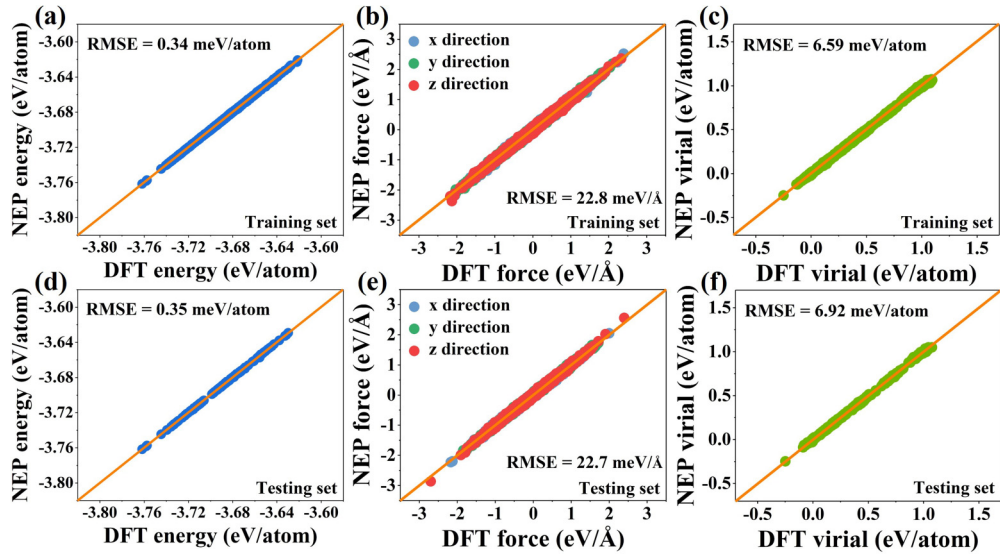


FIG. 7. (a),(d) Energy; (b),(e) force; and (c),(f) virial calculated from NEP compared with those calculated from DFT. The solid lines represent the identity function used to guide the eyes.

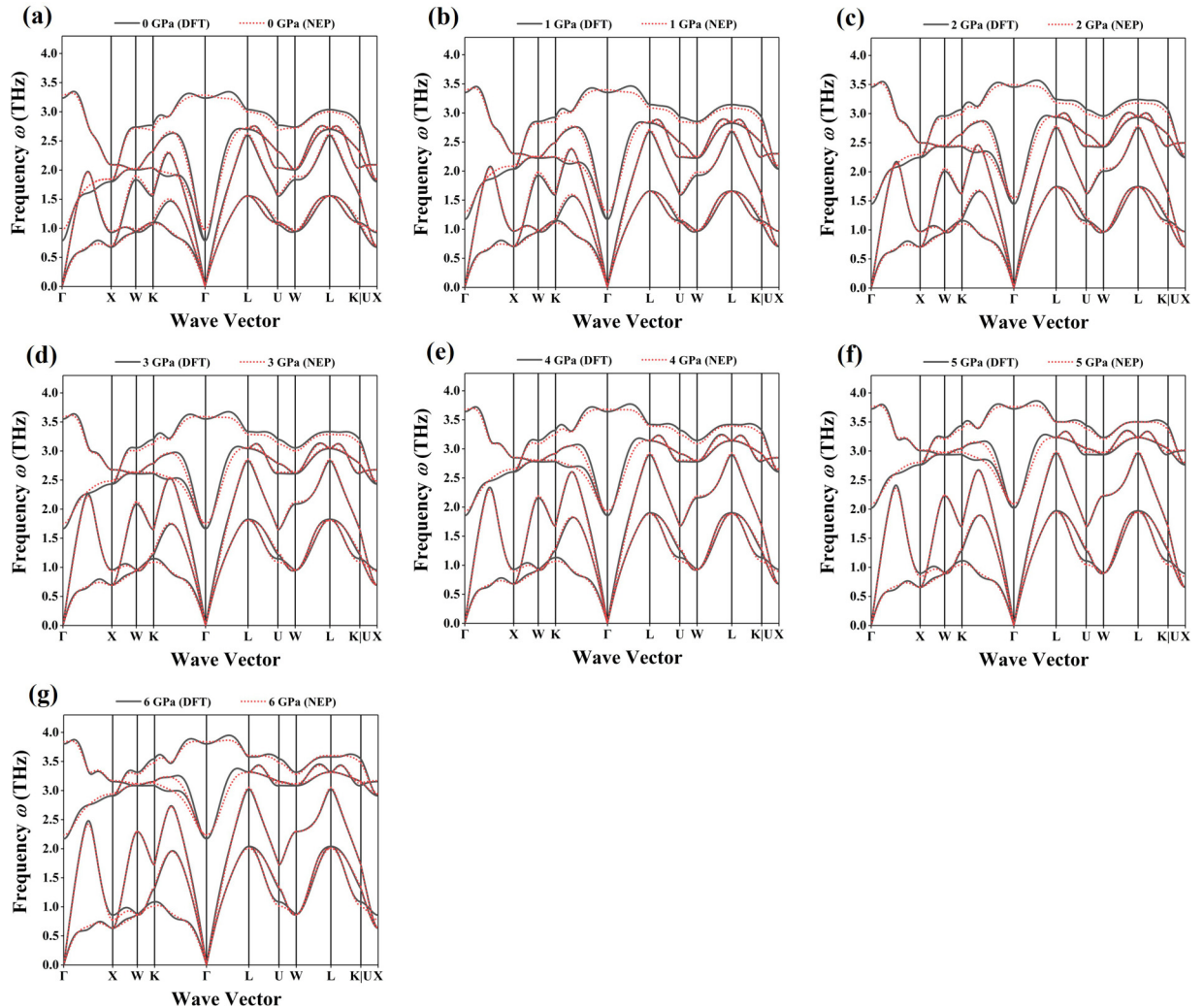


FIG. 8. Comparisons of harmonic phonon dispersions of PbTe under different pressures between DFT and NEP calculations.

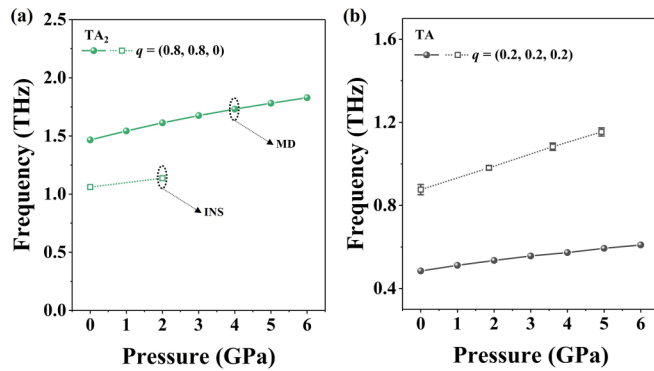


FIG. 9. Comparisons of experimental (hollow symbols) and theoretical (solid symbols) phonon frequencies for the (a) TA₂ mode at $q = (0.8, 0.8, 0)$ and the (b) TA mode at $q = (0.2, 0.2, 0.2)$.

pressure-dependent lattice dynamics of PbTe and provides an additional pressure dimension for regulating the thermal transport.

ACKNOWLEDGMENTS

This work is supported by the Research Grants Council of Hong Kong (Grants No. 17318122 and No. 17306721). The authors are grateful for the research computing facilities offered by ITS, HKU. X.S. and F.W. acknowledge support from the Helmholtz-OCPC Postdoc Program (ZD202029). We thank Markus Braden (Universität zu Köln) for assistance in the neutron scattering measurements performed at the LLB.

APPENDIX A: CONSTRUCTION OF A NEUROEVOLUTION MACHINE-LEARNING POTENTIAL

To train a machine-learning NEP [50,51], a $4 \times 4 \times 4$ supercell (128 atoms) was used to carry out *ab initio* molecular dynamics (AIMD) simulations to generate randomly displaced configurations at different temperatures (200, 300, 400, 500, 600, and 700 K) with triaxial strains ranging from -3% to 1% . The AIMD time step was set to 2 fs, and 3000 steps were conducted under each condition. The energy convergence threshold was set to 10^{-4} eV. We also included 25 configurations with randomly drawn displacements, as generated by the HIPHIVE package [52], to sample the low-temperature phase space of PbTe. There are totally 635 configurations obtained: 510 configurations for the training set and 125 configurations for the testing set. Accurate DFT calculations with a Γ -centering $3 \times 3 \times 3$ k -point mesh and a total energy tolerance of 10^{-8} eV were performed to extract energies, forces, and stresses. The radial and angular cutoffs of the NEP were chosen to be 9 and 7 Å, respectively. We applied 200 000 generations to achieve the converged results (Fig. 6).

The cross-validation results are shown in Fig. 7. The root-mean-square errors (RMSEs) of energies, forces, and virials for the training set are, respectively, 0.34 meV/atom, 22.8 meV/Å, and 6.59 meV/atom. The RMSEs of energies, forces, and virials for the testing set are 0.35 meV/atom, 22.7 meV/Å, and 6.92 meV/atom, respectively. The harmonic phonon dispersions along the high-symmetry paths calculated with our machine-learning NEP are comparable to that calcu-

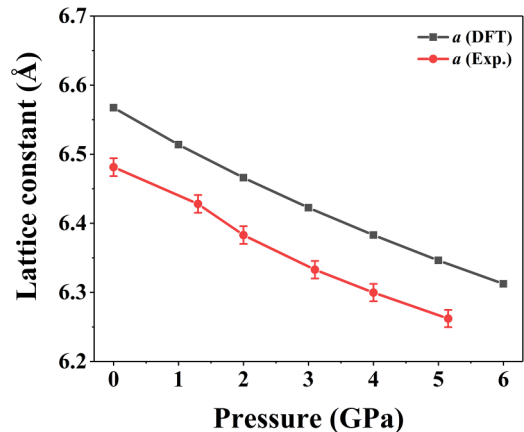


FIG. 10. Comparison of the experimental and DFT lattice constants of PbTe under different pressures.

lated from DFT (Fig. 8), suggesting high accuracy of our NEP. Figure 9 shows pressure-dependent phonon frequencies of the TA modes at q points of (0.8, 0.8, 0) and (0.2, 0.2, 0.2).

The measured and calculated lattice constants of PbTe under different pressures are shown in Fig. 10. It is seen that the calculated lattice constants slightly overestimate the experimental results.

APPENDIX B: HOMOGENEOUS NONEQUILIBRIUM MOLECULAR DYNAMICS

We used the HNEMD [46,47], as implemented in graphics processing units molecular dynamics (GPUMD) [35,36], to calculate the lattice thermal conductivity with a time step of 1 fs. To minimize the finite-size effect, we adopted $15 \times 15 \times 15$ conventional cells (27 000 atoms), which were firstly equilibrated in an NVT ensemble for 100 ps. HNEMD simulations were then performed in the NVT ensemble for 2.0 ns to extract the heat current. The targeted temperature was controlled by

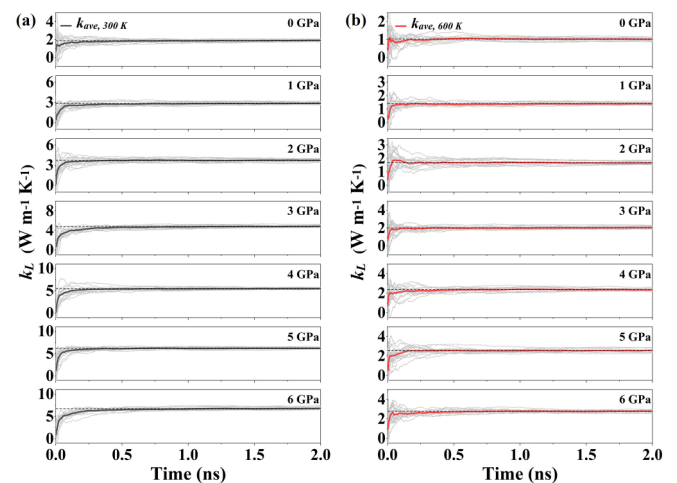


FIG. 11. Running average thermal conductivity of PbTe as a function of production time at (a) 300 K and (b) 600 K under different pressures. The light-gray lines represent 15 independent HNEMD simulations with different initial velocities. The black horizontal dashed lines are used to guide the eyes.

a Nosé-Hoover thermostat [53] and the coupling constant was set to 0.1 ps. The data were averaged over every 1000 steps before being recorded, and the driving force parameter was 10^{-4} \AA^{-1} . The spectral heat current data were sampled every 10 steps and the correlation time was 5 ps. Fifteen independent HNEMD simulations were carried out for each condition to

obtain the average lattice thermal conductivity and the related statistical error [Figs. 5(a) and 11]. The non-equilibrium heat flow obtained from the HNEMD simulation can be spectrally decomposed through the spectral heat current (SHC) method [46] without additional lattice dynamics calculations.

-
- [1] L. E. Bell, Cooling, heating, generating power, and recovering waste heat with thermoelectric systems, *Science* **321**, 1457 (2008).
- [2] Y. Pei, X. Shi, A. LaLonde, H. Wang, L. Chen, and G. J. Snyder, Convergence of electronic bands for high performance bulk thermoelectrics, *Nature (London)* **473**, 66 (2011).
- [3] M. Massetti, F. Jiao, A. J. Ferguson, D. Zhao, K. Wijeratne, A. Wurger, J. L. Blackburn, X. Crispin, and S. Fabiano, Unconventional thermoelectric materials for energy harvesting and sensing applications, *Chem. Rev.* **121**, 12465 (2021).
- [4] L. Zhang, X.-L. Shi, Y.-L. Yang, and Z.-G. Chen, Flexible thermoelectric materials and devices: From materials to applications, *Mater. Today* **46**, 62 (2021).
- [5] Y. Wu, P. Nan, Z. Chen, Z. Zeng, R. Liu, H. Dong, L. Xie, Y. Xiao, Z. Chen, H. Gu *et al.*, Thermoelectric enhancements in PbTe alloys due to dislocation-induced strains and converged bands, *Adv. Sci.* **7**, 1902628 (2020).
- [6] W. Li, Z. Chen, S. Lin, Y. Chang, B. Ge, Y. Chen, and Y. Pei, Band and scattering tuning for high performance thermoelectric $\text{Sn}_{1-x}\text{Mn}_x\text{Te}$ alloys, *J. Materiomics* **1**, 307 (2015).
- [7] Y. Wu, P. Nan, Z. Chen, Z. Zeng, S. Lin, X. Zhang, H. Dong, Z. Chen, H. Gu, W. Li *et al.*, Manipulation of band degeneracy and lattice strain for extraordinary PbTe thermoelectrics, *Research* **2020**, 8151059 (2020).
- [8] H.-T. Liu, Q. Sun, Y. Zhong, C.-L. Xia, Y. Chen, Z.-G. Chen, and R. Ang, Achieving high-performance n-type PbTe via synergistically optimizing effective mass and carrier concentration and suppressing lattice thermal conductivity, *Chem. Eng. J.* **428**, 132601 (2022).
- [9] Y. Xiao, H. Wu, J. Cui, D. Wang, L. Fu, Y. Zhang, Y. Chen, J. He, S. J. Pennycook, and L.-D. Zhao, Realizing high performance n-type PbTe by synergistically optimizing effective mass and carrier mobility and suppressing bipolar thermal conductivity, *Energy Environ. Sci.* **11**, 2486 (2018).
- [10] A. A. El-Sharkawy, A. M. A. El-Azm, M. I. Kenawy, A. S. Hillal, and H. M. Abu-Basha, Thermophysical properties of polycrystalline PbS, PbSe, and PbTe in the temperature range 300–700 K, *Int. J. Thermophys.* **4**, 261 (1983).
- [11] E. S. Toberer, A. Zevkink, and G. J. Snyder, Phonon engineering through crystal chemistry, *J. Mater. Chem.* **21**, 15843 (2011).
- [12] A. J. Miller, G. A. Saunders, and Y. K. Yagurtcu, Pressure dependences of the elastic constants of PbTe, SnTe and $\text{Ge}_{0.08}\text{Sn}_{0.92}\text{Te}$, *J. Phys. C: Solid State Phys.* **14**, 1569 (1981).
- [13] S. Klotz, Phonon dispersion curves by inelastic neutron scattering to 12 GPa, *Z. Krist.-Cryst. Mater.* **216**, 420 (2001).
- [14] O. Delaire, J. Ma, K. Marty, A. F. May, M. A. McGuire, M.-H. Du, D. J. Singh, A. Podlesnyak, G. Ehlers, M. Lumsden *et al.*, Giant anharmonic phonon scattering in PbTe, *Nat. Mater.* **10**, 614 (2011).
- [15] T. Shiga, J. Shiomi, J. Ma, O. Delaire, T. Radzynski, A. Lusakowski, K. Esfarjani, and G. Chen, Microscopic mechanism of low thermal conductivity in lead telluride, *Phys. Rev. B* **85**, 155203 (2012).
- [16] T. Shiga, T. Murakami, T. Hori, O. Delaire, and J. Shiomi, Origin of anomalous anharmonic lattice dynamics of lead telluride, *Appl. Phys. Express* **7**, 041801 (2014).
- [17] S. Lee, K. Esfarjani, T. Luo, J. Zhou, Z. Tian, and G. Chen, Resonant bonding leads to low lattice thermal conductivity, *Nat. Commun.* **5**, 3525 (2014).
- [18] S. Ju, T. Shiga, L. Feng, and J. Shiomi, Revisiting PbTe to identify how thermal conductivity is really limited, *Phys. Rev. B* **97**, 184305 (2018).
- [19] Y. Xia, Revisiting lattice thermal transport in PbTe: The crucial role of quartic anharmonicity, *Appl. Phys. Lett.* **113**, 073901 (2018).
- [20] K. M. O. Jensen, E. S. Božin, C. D. Malliakas, M. B. Stone, M. D. Lumsden, M. G. Kanatzidis, S. M. Shapiro, and S. J. L. Billinge, Lattice dynamics reveals a local symmetry breaking in the emergent dipole phase of PbTe, *Phys. Rev. B* **86**, 085313 (2012).
- [21] C. W. Li, O. Hellman, J. Ma, A. F. May, H. B. Cao, X. Chen, A. D. Christianson, G. Ehlers, D. J. Singh, B. C. Sales, and O. Delaire, Phonon Self-Energy and Origin of Anomalous Neutron Scattering Spectra in SnTe and PbTe Thermoelectrics, *Phys. Rev. Lett.* **112**, 175501 (2014).
- [22] C. W. Li, J. Ma, H. B. Cao, A. F. May, D. L. Abernathy, G. Ehlers, C. Hoffmann, X. Wang, T. Hong, A. Huq *et al.*, Anharmonicity and atomic distribution of SnTe and PbTe thermoelectrics, *Phys. Rev. B* **90**, 214303 (2014).
- [23] Y. Chen, X. Ai, and C. A. Marianetti, First-Principles Approach to Nonlinear Lattice Dynamics: Anomalous Spectra in PbTe, *Phys. Rev. Lett.* **113**, 105501 (2014).
- [24] G. A. S. Ribeiro, L. Paulatto, R. Bianco, I. Errea, F. Mauri, and M. Calandra, Strong anharmonicity in the phonon spectra of PbTe and SnTe from first principles, *Phys. Rev. B* **97**, 014306 (2018).
- [25] Z. Li, S. Li, J.-P. Castellan, R. Heid, Y. Xiao, L.-D. Zhao, Y. Chen, and F. Weber, Anomalous transverse optical phonons in SnTe and PbTe, *Phys. Rev. B* **105**, 014308 (2022).
- [26] A. H. Romero, E. K. U. Gross, M. J. Verstraete, and O. Hellman, Thermal conductivity in PbTe from first principles, *Phys. Rev. B* **91**, 214310 (2015).
- [27] Y. Lu, T. Sun, and D.-B. Zhang, Lattice anharmonicity, phonon dispersion, and thermal conductivity of PbTe studied by the phonon quasiparticle approach, *Phys. Rev. B* **97**, 174304 (2018).
- [28] Z. Zeng, C. Zhang, Y. Xia, Z. Fan, C. Wolverton, and Y. Chen, Nonperturbative phonon scatterings and the two-channel thermal transport in Tl_3VSe_4 , *Phys. Rev. B* **103**, 224307 (2021).

- [29] W. Setyawan and S. Curtarolo, High-throughput electronic band structure calculations: Challenges and tools, *Comput. Mater. Sci.* **49**, 299 (2010).
- [30] G. Kresse and J. Furthmüller, Efficient iterative schemes for *ab initio* total-energy calculations using a plane-wave basis set, *Phys. Rev. B* **54**, 11169 (1996).
- [31] G. Kresse and D. Joubert, From ultrasoft pseudopotentials to the projector augmented-wave method, *Phys. Rev. B* **59**, 1758 (1999).
- [32] J. P. Perdew, K. Burke, and M. Ernzerhof, Generalized Gradient Approximation Made Simple, *Phys. Rev. Lett.* **77**, 3865 (1996).
- [33] D.-B. Zhang, T. Sun, and R. M. Wentzcovitch, Phonon Quasiparticles and Anharmonic Free Energy in Complex Systems, *Phys. Rev. Lett.* **112**, 058501 (2014).
- [34] A. Carreras, A. Togo, and I. Tanaka, DynaPhoPy: A code for extracting phonon quasiparticles from molecular dynamics simulations, *Comput. Phys. Commun.* **221**, 221 (2017).
- [35] Z. Fan, W. Chen, V. Vierimaa, and A. Harju, Efficient molecular dynamics simulations with many-body potentials on graphics processing units, *Comput. Phys. Commun.* **218**, 10 (2017).
- [36] Z. Fan, Y. Wang, P. Ying, K. Song, J. Wang, Y. Wang, Z. Zeng, K. Xu, E. Lindgren, J. M. Rahm *et al.*, GPUMD: A package for constructing accurate machine-learned potentials and performing highly efficient atomistic simulations, *J. Chem. Phys.* **157**, 114801 (2022).
- [37] F. Weber, Y. Chen, A. Ivanov, S. Klotz, Z. Li, and L. Powalla, Anharmonic lattice dynamics under pressure in PbTe (2019), doi:10.5291/ILL-DATA.7-01-468.
- [38] F. Weber, A. Ivanov, S. Klotz, Z. Li, and X. Shen, Anharmonic lattice dynamics in thermoelectric PbTe under high pressure (2021), doi:10.5291/ILL-DATA.7-01-552.
- [39] S. Klotz, *Techniques in High Pressure Neutron Scattering* (CRC Press/Taylor & Francis, Boca Raton, 2012).
- [40] O. I. Siidra, E. V. Nazarchuk, D. O. Charkin, N. V. Chukanov, A. Y. Zakharov, S. N. Kalmykov, Y. A. Ikhlaynen, and M. I. Sharikov, Open-framework sodium uranyl selenate and sodium uranyl sulfate with protonated morpholino-N-acetic acid, *Z. Kristall. - Cryst. Mater.* **234**, 109 (2019).
- [41] K. Komatsu, S. Klotz, A. Shinozaki, R. Iizuka, L. E. Bove, and H. Kagi, Performance of ceramic anvils for high pressure neutron scattering, *High Press. Res.* **34**, 494 (2014).
- [42] We note that the pressure cell used at ILL was so far only employed for neutron diffraction experiments, and the observed strongly temperature-dependent background scattering as a function of neutron energy transfer is now subject to further investigation.
- [43] B. Mozer, K. Otnes, and H. Palevsky, in *Lattice Dynamics*, edited by R. F. Wallis (Pergamon, Oxford, 1965), p. 63.
- [44] O. L. Anderson and R. C. Liebermann, Equations for the elastic constants and their pressure derivatives for three cubic lattices and some geophysical applications, *Phys. Earth Planet. Inter.* **3**, 61 (1970).
- [45] L. Xu, Y. Zheng, and J.-C. Zheng, Thermoelectric transport properties of PbTe under pressure, *Phys. Rev. B* **82**, 195102 (2010).
- [46] Z. Fan, H. Dong, A. Harju, and T. Ala-Nissila, Homogeneous nonequilibrium molecular dynamics method for heat transport and spectral decomposition with many-body potentials, *Phys. Rev. B* **99**, 064308 (2019).
- [47] D. J. Evans, Homogeneous NEMD algorithm for thermal conductivity'application of non-canonical linear response theory, *Phys. Lett. A* **91**, 457 (1982).
- [48] A. J. Gabourie, Z. Fan, T. Ala-Nissila, and E. Pop, Spectral decomposition of thermal conductivity: Comparing velocity decomposition methods in homogeneous molecular dynamics simulations, *Phys. Rev. B* **103**, 205421 (2021).
- [49] M. Simoncelli, N. Marzari, and F. Mauri, Unified theory of thermal transport in crystals and glasses, *Nat. Phys.* **15**, 809 (2019).
- [50] Z. Fan, Z. Zeng, C. Zhang, Y. Wang, K. Song, H. Dong, Y. Chen, and T. Ala-Nissila, Neuroevolution machine learning potentials: Combining high accuracy and low cost in atomistic simulations and application to heat transport, *Phys. Rev. B* **104**, 104309 (2021).
- [51] Z. Fan, Improving the accuracy of the neuroevolution machine learning potential for multi-component systems, *J. Phys.: Condens. Matter* **34**, 125902 (2022).
- [52] F. Eriksson, E. Fransson, and P. Erhart, The Hiphive package for the extraction of high-order force constants by machine learning, *Adv. Theory Simul.* **2**, 1800184 (2019).
- [53] M. Tuckerman, *Statistical Mechanics: Theory and Molecular Simulation*, Oxford Graduate Texts (Oxford University Press, Oxford, 2010).